Z. Liang, Z. Yu, H. Liu, L. Chen, X. Huang (2022) Combustion and Emission Characteristics of a Compression Ignition Engine burning a Wide Range of Conventional Hydrocarbon and Alternative Fuels, **Energy**, 250, 123717. https://doi.org/10.1016/j.energy.2022.123717

Combustion and Emission Characteristics of a Compression Ignition Engine burning a Wide Range of Conventional Hydrocarbon and Alternative Fuels

Zhirong Liang [a,b], Zhenhong Yu [c], Haoye Liu [d*], Longfei Chen [e*], Xinyan Huang [b]

[a] *Interdisciplinary Division of Aeronautical and Aviation Engineering, The Hong Kong Polytechnic University, Hong Kong, 999077, China*

[b] *Department of Building Environment and Energy Engineering, The Hong Kong Polytechnic University, Hong Kong, 999077, China*

[c] *Hudson River Research, LLC, 123 Town Square Place, Jersey City, New Jersey, 07310, USA*

[d] *School of Mechanical Engineering, Tianjin University, Tianjin 300073, China*

[e] *School of Energy and Power Engineering, Beihang University, Beijing, 100191, China*

* Both Longfei Chen (chenlongfei@buaa.edu.cn) and Haoye Liu (liuhaoyebirmingham@gmail.com) as corresponding authors, have equal contributions to this work.

Abstract

General aviation aircraft driven by aviation piston engines (APE) have gained a broad range of applications. Aviation fuels blended with long-chain alcohols is a promising means for APE to mitigate its dependency on fossil fuel. Herein, the combustion and emission characteristics of an aviation compression ignition engine burning a baseline diesel, the RP-3 kerosene, and a synthetic Fischer-Tropsch (FT) fuel were analyzed. The engine tests were carried out under different conditions via varying pentanol additive ratio (PAR), fuel injection timing and engine load variables. The Response Surface Method (RSM) was utilized to quantify the effectiveness of independent variables on the target responses of indicated thermal efficiency (ITE), nitrogen oxides (NOx) and particulate matter (PM) emissions. Compared to the baseline diesel, burning the pentanol-FT blends (40% PAR) significantly reduces NOx by 81% and PM by 75% with a prominent increase of ITE by 7.2%. Based on the analysis of variance, the RSM-derived model demonstrated that the fuel type predominantly determines ITE and NOx, while PAR primarily alters PM emissions. The binary effects of independent variables on the target responses were further resolved quantitatively. Moreover, the RSM was well validated to implement effective prediction on the engine performance/emission characteristics.

Keywords: Aviation compression ignition engine, Synthetic FT fuel, RP-3 kerosene, Pentanol, Combustion and emissions, RSM prediction.

Nomenclatures

A	in-cylinder wall surface [m^2]	’	corrected value
h	convective heat transfer coefficient [W m^{-2} K^{-1})]	—	value by average
L	higher latent heat		
$H0$	null hypothesis	*Abbreviation*	
Hu	lower heating value [J kg^{-1}]	ANOVA	analysis of variance
K	number of group	APE	aviation piston engines
m	mass flow rate [kg s^{-1}]	BTDC	before top dead center
N	overall sample size	CA	crank angle
n	number of samples	CI	compression ignition
p	in-cylinder pressure [bar]	CN	cetane number
T	temperature [K]	CO	carbon oxide
Q	heat [J]	DF	degree of freedom
V	volume [m^3]	DoE	design of experiments
W	work [W]	ECU	electronic-control-unit
Y	target responses	FT	fischer-tropsch
		GA	general aircraft
Greek		UHC	unburnt hydrogen carbon
ρ	density [kg m^{-3}]	HRR	heat release rate
θ	crack angle [°]	IC	internal combustion
γ	specific heat ratio [-]	IMEP	indicated-mean-effective-pressure
η	efficiency [%]	ISFC	indicated specific fuel consumption
		ITE	indicated thermal efficiency
Subscripts		LHV	lower heating value
c	convective heat transfer or combustion	NOx	nitrogen oxides
f	fuel	PAR	pentanol additive ratio
g	gas	PM	particulate matter
i	indicated / indicator	RCCI	reactivity controlled compression ignition
j	indicator	RP-3	rocket propellant - 3
n	net	RPM	revolutions per minute
r	replicate measurements	RSM	response surface method
w	Wall	RSS	residual sum of squares
ws	with specific parameter	SI	spark ignition
wos	without specific parameter	SMD	Sauter mean diameter
		SOI	start of injection
Superscript		TDC	top dead center
°	Degree	UAV	unmanned aerial vehicles

1. Introduction

Aircraft powered by aviation piston engines (APE) are broadly utilized in the field of General Aviation (GA). By the end of 2016, commercial aircraft fleet data (Airbus 2017) showed that nearly 20,000 GA aircraft were in service globally, and it increased dramatically to be 446,000 by 2018 (GAMA 2018), which have adverse impacts on airport local air quality [1, 2]. An assessment undertaken by the Swiss Federal Office of Civil Aviation (FOCA) demonstrated that the role of GA aircraft in total aviation fuel consumption accounted for less than 3% of total aviation fuel consumption, whereas its contributions to entire aviation-generated carbon monoxide (CO), unburnt hydrocarbon (UHC) and nitrogen oxide (NOx) were over 39%, 11% and 9%, respectively [3]. Particulate matter (PM) emissions from aviation are characterized by particle size below 100 nm, which is able to penetrate deep into human lungs and bloodstreams and cause cardiovascular and nervous impairments [4]. The GA-emitted PMs include soot particles and organic species that can form secondary organic aerosols (SOA) near airports, which thus deteriorate local air quality [5, 6]. In terms of military aircraft, their PM emissions could severely ruin the training and combat missions owing to the increase of infrared visibility of particulates [7].

Many previous studies have characterized the PM emissions from aviation gas turbine engines, while few of them addressed the PM characteristics of APE [6, 8]. Recently, Chen et al. [9] reported that an aviation CI engine burning RP-3 generated lower soot emissions by approximately one order of magnitude than burning diesel at high engine loads. However, they did not characterize the PM emissions from the same engine burning alternative fuels (e.g. the popular Fischer-Tropsch fuel). Even though the total fuel consumption of APE is much less than those of turbofan aircraft engines, the emissions from APE were substantial because of the intrinsic low thermodynamic efficiency of the reciprocating piston engines [10]. Therefore, it would be desirable to investigate combustion performance and emission characteristics of the APE to seek a proper mitigation strategy for GA activities.

In general, there are two combustion modes for APE, spark ignition (SI) and compression ignition (CI). APE has mainly used the SI mode to burn light fuels (gasoline) for decades. For the sake of reliability, stability, simplified logistic and fuel economy, the APE with the CI mode that burns heavy fuels (light diesel or kerosene) is considered as a promising propulsion technology. Thus, it can be used in fixed wing aircraft, helicopters, and unmanned aerial vehicles (UAV) for civil and military applications [3, 10]. In addition, a “single fuel forward” policy using the aviation kerosene, JP-8, has been adopted by the NATO and US Army [11, 12]. Therefore, the trend of adopting heavy fuels in APE with the CI mode becomes more prevailing now for both military and civil aircraft.

Aviation alternative fuels (SAFs) have gained increasing demands during recent years, to reduce the dependence of aviation on fossil fuels [13]. One of the major SAFs is the synthetic Fischer-Tropsch (FT) fuel, and the process and the adoption of the FT fuels have the following advantages: 1) it can be produced from various carbon-based resources such as natural gas, coal, or biomass; 2) the production processes are efficient to potentially decentralize energy resources among the global energy markets; 3) the application of FT fuel is capable of mitigating the aircraft emissions [12, 14]. The ‘iso-paraffinic kerosene’ FT fuel was initially produced by Sasol in South Africa, and was allowed in aviation by blending up to 50% (volume

fraction) in aviation Jet A-1 fuel in 1999 [15]. In the past decade, the U.S. military F-22, F-15 and F-11 aircraft have been certified on the adoption of the FT blends, approved by ASTM D7566 specification [16]. Nowadays, FT fuel is becoming commercially feasible for aviation power generation, ground transportation with respect to energy sustainable development [4].

Many of previous studies have been focused on the analysis of the FT fuels that are mainly adopted in gas turbine engines. For instance, the turboshaft (T63) and turbofan (CFM56-7B, CFM56-2C, F117, PW308 and PW1000) gas turbine engines were comprehensively studied under the US Air Force sponsored programs to evaluate the impacts of burning the FT fuels and the FT/JP-8 blends on the engine emissions [17]. Up to date, few literatures have analyzed the emission characteristics of the FT fuels implemented in APE. In this study, except for the FT fuel, a rocket propellant - 3 (RP-3) kerosene is also analyzed since it is the most widely used aviation kerosene in the Chinese market. The physiochemical characteristics of the RP-3 kerosene are significantly different from the Jet-A/JP-8 series, in terms of aromatic hydrocarbon content and flash point [18].

Fuel additives, particularly oxygen-contained additives like alcohols, have gained increasing usage in internal combustion (IC) engines for years, owing to their superior capability of inhibiting pollutants formation [19, 20]. In terms of burning alcohol-blended fuels in IC engines, previous studies have emphasized on short-chain alcohols (e.g. methanol, ethanol and propanol with carbon number < 4) [21, 22]. The long-chain alcohols (e.g. pentanol with 5-carbon chain structure) have recently been found to be more promising alcohol candidates than short-chain alcohols, due to their higher energy density, higher cetane number (CN), larger heating value, and better miscibility with conventional hydrocarbon fuels (e.g. diesel fuel) than the short-chain alcohol, [23, 24]. Like ethanol, the long-chain alcohols can be produced via alcoholic fermentation of biomass feedstocks, so they are renewable fuels with less carbon footprint [25]. Nevertheless, few studies were carried out to investigate the effect of long-chain alcohols on IC engine combustions. Therefore, the effects of blending long-chain alcohols as CI engine fuels, particularly as they are blended with heavy aviation fuels, are still not fully understood. Additionally, the fuel oxygen content increases linearly with increasing alcohol drop-in ratio, by which engine performances, especially emission characteristics, are strongly affected [26]. For different base fuels with various properties, the effects of blending long-chain alcohols may be diverse.

Besides the fuel properties, engine control variables (engine load, injection timing, etc.) also affect the in-cylinder combustion process and the resulting engine performance [27, 28]. For conventional diesel engine combustion mode, advanced injection timing has been proved to be able to decrease hydrocarbon, CO and soot emissions, and to increase NOx emissions. The best thermal efficiency is found at an intermedium injection timing [27]. However, the influence from engine control variables could be complicated if the fuel properties are not the same as the standard diesel fuel [29, 30]. Thus, it is necessary to find the relationship between the independent variables such as fuel injection timing, fuel types, pentanol drop-in ratio and engine load and the key responses like indicated thermal efficiency (ITE), nitrogen oxides (NOx) and PM emissions via a dedicate engine study. It is also necessary to find the optimum variables to achieve satisfactory engine performance in combustion and emission characteristics.

This work explores the effect of three conventional and alternative fuels: a baseline diesel, aviation RP-3

kerosene, and a synthetic FT fuel, as well as their mixtures with different pentanol blending ratios, on the combustion and emission characteristics of an aviation CI engine under various engine conditions. The response surface method (RSM) of the Design of Experiments (DoE) has been adopted for exploring the relationships between the influencing variables and the key responses. RSM, which has been utilized in many research areas, can evaluate the relationship between the response and the independent variables, and is capable of optimizing the response surface function and predicting the future response [31, 32]. For instance, Chen et al. [33]. used the historical data design under RSM to formulate the correlation between the fuel spray Sauter mean diameter (SMD) and the main physical factors including viscosity, fuel injection pressure, air-blast pressure. Li et al. [34] proved the robustness of design using RSM to model and optimize the gap-graded cement paste blended with supplementary cementitious materials. In this study, by using RSM combined with the analysis of variance (ANOVA), the binary and interactive effects of different variables on the engine performance/emission characteristics were quantitatively resolved to find supreme alternative aviation fuels. Moreover, the predictive effectiveness of the RSM model on the corresponding engine responses has been evaluated.

2. Experiments

2.1 Engine test system

This work was conducted on a one-cylinder (modified from four cylinders) aviation compression ignition engine assembled with a common rail direct injection system. The operation of the test engine was implemented by an open electronic-control unit (ECU) via a customer-designed Labview program [35]. The schematic of the engine test rig with sampling unit is illustrated in Fig. 1, and the engine specifications are provided in Table 1. To study the impact of the operational variables and fuel additives on the engine combustion and emission characteristics, formal engine tests were carried out, the start of injection (SOI) timing was adjusted to sweep among the four test points of 16, 18, 19 and 21 crank angle degree (°CA) before top dead center (BTDC); engine load was regulated from low to high values at the four test conditions of 2, 4, 6, 8 bar indicated-mean-effective-pressure (IMEP); and pentanol additive ratio (PAR) was varied at four test ratios of 0%, 15%, 30% and 40% (by volume) for all the test fuels, respectively.

The other engine operating variables were remained unchanged, as the injection pressure at 75 MPa and the engine speed at 1600 revolutions per minute (RPM) throughout all the tests. Moreover, a split injection methodology (primary injection + main injection) was implemented (as seen further in Section 3.1). The fuel mass ratio of the primary injection to the total injections was maintained at around 12%. Besides, the interval of main and primary injection was remained constant by 15 °CA, and the duration of the main injection was regulated to attain the target load. Moreover, a series of validation engine tests were further carried out, and the test purpose was to verify the prediction effect of RSM model constructed. To facilitate error analysis, each formal engine test was repeated three times, while each validation engine test was repeated twice. Details of engine operational strategies are provided in Table 2.

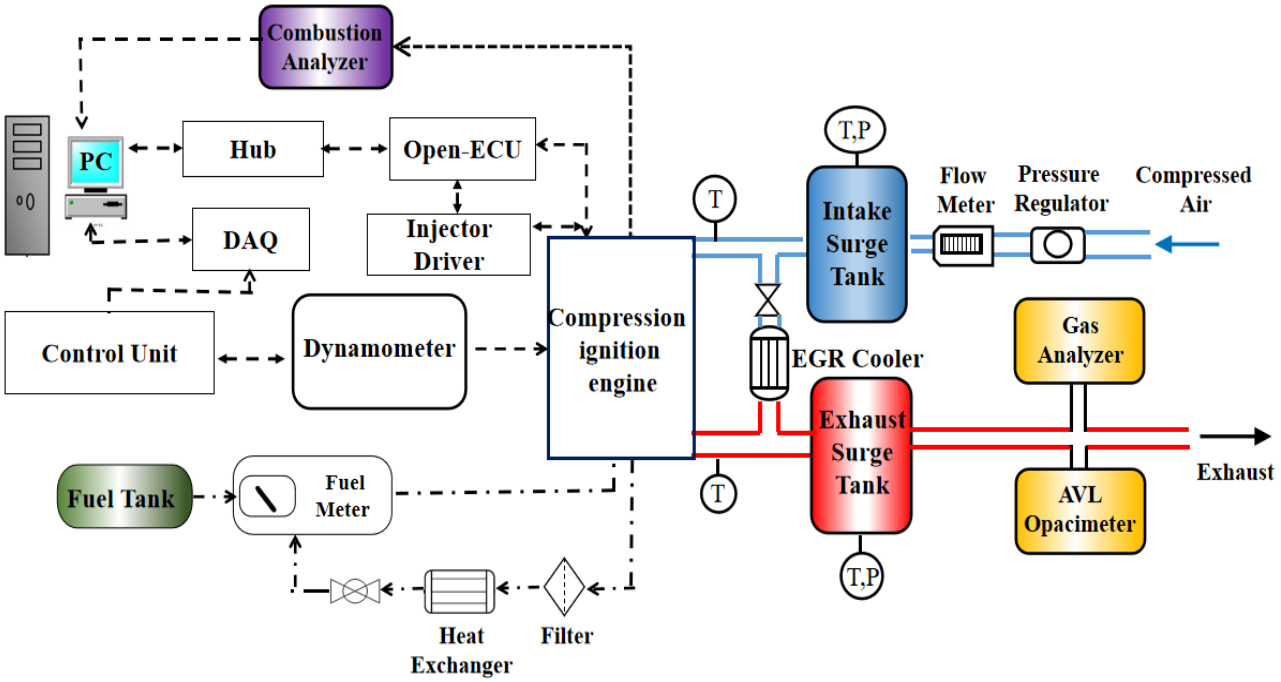

Figure 1. The schematic of engine test rig with sampling unit.

Table 1. Engine specifications.

Engine	Single cylinder four-stroke engine
Compression Ratio	16.7:1
Displacement	0.5 L
Bore / Stroke / Connecting rod length	83.1 / 92 / 145.8 mm
Injection system	Direct injection common rail
Injector holes	7 Holes, 0.136 mm diameter
Swirl ratio	1.7

Table 2. Engine operational conditions.

Formal engine tests	
Fuel types	Diesel / RP-3 / FT
SOI	16 °CA, 18 °CA, 19 °CA, 21 °CA BTDC
PAR	0%, 15%, 30%, 40%
Injection strategy	Main plus primary injections (primary injection ratio ~12%)
Injection pressure	75 MPa
Engine speed	1600 RPM
Engine load	2, 4, 6, 8 bar IMEP
Validation engine tests (@ 8 bar IMEP Engine load)	Fuel types (Diesel, RP-3, FT) × SOI (17, 20 °CA BTDC) × PAR (10%, 35%)

For each engine test, the in-cylinder pressure was monitored by a piezo electric pressure sensor, while the crankshaft angle was encoded by an optical shaft encoder. The heat release rate (HRR) was obtained based on the following calculations:

$$\frac{dQ_g}{d\theta} = \frac{dQ_n}{d\theta} + \frac{Q_w}{d\theta} \quad \text{Eq. (1)}$$

$$\frac{dQ_n}{d\theta} = \frac{\gamma}{\gamma-1} p \frac{dV}{d\theta} + \frac{1}{\gamma-1} V \frac{dp}{d\theta} \quad \text{Eq. (2)}$$

$$\frac{dQ_w}{d\theta} = \frac{A_w h_c (T - T_w)}{6n} \quad \text{Eq. (3)}$$

where $\frac{dQ_n}{d\theta}$and $\frac{dQ_w}{d\theta}$ denote the net HRR and the heat loss rate against crank angle (CA); V and p denote the cylinder volume and the in-cylinder pressure; T and T_w denote the in-cylinder gas mean temperature and wall temperature; γ is the specific heat ratio of air, A_w is the in-cylinder wall surface, h_c is the effective coefficient for convective heat transfer, and θ represents CA. Moreover, indicated thermal efficiency (ITE - η_i) was obtained by:

$$\eta_i = \frac{W_i}{m_f \times Hu_f} \quad \text{Eq. (4)}$$

where W_i represents the indicated engine work, and m_f and Hu_f represent the fuel flow rate and the fuel lower heating value.

Since the lower heating values (*LHV*) of the three test fuels are different, the fuel usage of the test fuels and their pentanol blends need to be corrected to reflect the total energy consumed with diesel as baseline [35]:

$$m'_{\text{RP-3/FT}} = m_{\text{RP-3/FT}} \times \frac{LHV_{\text{RP-3/FT}}}{LHV_{\text{diesel}}} \quad \text{Eq. (5)}$$

where $m'_{\text{RP-3/FT}}$ are the corrected fuel usage of RP-3/FT; $m_{\text{RP-3/FT}}$represents the actual fuel consumption of RP-3/FT; $LHV_{\text{RP-3/FT}}$ and LHV_{diesel} represent the lower heating values of RP-3/FT, and baseline diesel.

$$m'_{\text{new}} = m_{\text{measure}} \times \frac{V_{\text{diesel/RP-3/FT}} \times \rho_{\text{diesel/RP-3/FT}} \times LHV_{\text{diesel/RP-3/FT}} + V_{\text{pentanol}} \times \rho_{\text{pentanol}} \times LHV_{\text{pentanol}}}{V_{\text{diesel/RP-3/FT}} \times \rho_{\text{diesel/RP-3/FT}} + V_{\text{pentanol}} \times \rho_{\text{pentanol}}} \times LHV_{\text{diesel}} \quad \text{Eq. (6)}$$

where m'_{new} and m_{measure} represent the corrected fuel consumption and the measured fuel consumption, respectively; $V_{\text{diesel/RP-3/FT}}$ and V_{pentanol} are the volume percentages of the diesel/RP-3/FT and pentanol in the mixing fuels, respectively; $\rho_{\text{diesel/RP-3/FT}}$ and ρ_{pentanol} are the densities of diesel/RP-3/FT and pentanol, respectively. The fuel consumption of the RP-3/FT and blended fuels have been processed in correction referred to baseline diesel fuel accordingly. Note that the crank angle interval between the SOI and CA10 (combustion phase of 10% burning point) is defined as ignition delay, while the crank angle interval between CA10 and CA90 (combustion phase of 90% burning point) is defined as combustion duration.

Error analysis for engine measurements and analyses, such as in-cylinder pressure, ITE was performed using the root mean square function:

$$U_R = \left[\left(\frac{\partial R}{\partial x_1 \times U_{x_1}}\right)^2 + \left(\frac{\partial R}{\partial x_2 \times U_{x2}}\right)^2 + \cdots + \left(\frac{\partial R}{\partial x_n \times U_{x_n}}\right)^2\right]^{\frac{1}{2}} \quad \text{Eq. (7)}$$

where U_R is the uncertainty of the calculated quantity R; x_n is the measured uncertainties of the N^{th} independent variable; Ux_n is the uncertainty of x_n caused by the facilities, shown in Table 3.

Table 3. Uncertainties of the measured and calculated parameters.

	Parameters	Uncertainty (%)	Resolution
Measured parameters	Engine speed	0.5	1 rpm
	Engine load	0.5	0.01 bar
	Crank angle	0.1	0.01 °CA
	Intake pressure	0.1	1 kPa
	Intake temperature	1.0	0.1 K
	Fuel flow meter	1.0	0.01 kg/h
	Gaseous analyzer	0.5	1 ppm
	Soot opacity	1.0	0.001/m
	Air flow meter	1.0	0.1 m^3/h
Calculated parameters	In-cylinder pressure	0.5	NA
	ITE	0.8	NA
	IMEP	0.6	NA

2.2 Fuel properties

Table 4 lists the physical properties of the synthetic FT fuel, RP-3 kerosene, diesel and pentanol additive. Moreover, the properties of FT/RP-3/diesel blended with pentanol in different ratios of 15%, 30% and 40% by volumes were calculated according to the method provided in previous literature [36, 37]. This method determines the blending properties based on the basic features incorporation of the neat fuels (Fuel blends properties are provided in SI - S1). RP-3 kerosene and FT fuel have both lower carbon number and CN than the baseline diesel. Meanwhile, owing to having lower surface tension and kinetic viscosity, RP-3 kerosene and FT fuel has better evaporation and atomization characteristics than the baseline diesel. Pentanol has 18.2% oxygen content, lower CN, and higher latent heat. Moreover, since both FT fuel and pentanol contains no sulfur and aromatic contents, the pentanol addition into the test fuels (baseline diesel and RP-3 kerosene) will decrease concentrations of such compounds compared to the neat fuels.

Table 4. Neat fuel properties.

Fuel types	Diesel	RP-3	FT	Pentanol
Chemical formula	C16-C23	C8-C12	C7-C11	C5H12O
Density (kg/L, 20℃)	0.83	0.79	0.78	0.82
Cetane number	56.5	42.0	40.2	22.5
Latent heat (kJ/kg, 25 ℃)	270	282	291	308
Lower heating value (MJ/kg)	42.68	43.43	42.10	35.06
Kinetic viscosity (mm^2/s, 20 ℃)	4.13	1.28	1.16	2.89
Oxygen content (wt %)	0	0	0	18.2
Surface tension (N/m, 20℃)	$27.5x10^{-3}$	$23.60\ x10^{-3}$	$21.4\ x10^{-3}$	$24.7\ x10^{-3}$
Sulfur (wt %)	0.50	0.30	0	0
Aromatic (vol %)	23.3	19.0	0	0
Boiling point (℃)	T10 = 223 T50 = 266 T90 = 311	T10 = 172.8 T50 = 194.9 T90 = 224.4	T10 = 163.2 T50 = 185.9 T90 = 212.0	138

2.3. Exhaust sampling system

As for the exhaust sampling system, a gaseous emissions bench (CEBII, AVL) comprised of a NOx analyzer was deployed to measure the NOx emissions. Meanwhile, the soot emissions were measured by an Opacimeter (Model 439, AVL). The specific quantity of particles (PM) obtained by the Opacimeter was based on the calculations using the Beer-Lambert law, which relates the light attenuation by the light-absorbing soot particles. The particle opacity (soot opacity) measured by the Opacimeter is proportional to the particle mass fractions (soot mass). Before entering the measurement instruments, the exhaust samples were transferred via a heated line with a constant temperature of 190℃ to avoid water condensation, and then an in-house built diluter with the dilution factor controlled at 10:1 (dilution by dry and particle-free compressed air at ambient temperature). The arrangement of this sampling system can be found in our previous publication elsewhere [4].

2.4 Response Surface Method in Design of Experiment with ANOVA analysis

The Design of Experiments method (DoE) has been employed to investigate the cause-effect relationship between the engine operational variables and the target responses [32]. The DoE approach has various applications in many research areas, since it can implement reliable statistic analysis that processes planning, conducting, and interpreting controlled experiments to assess the impact of the investigated variables on influencing the value of target responses [31]. In other words, it allows for multiple input variables to be manipulated, and reflect their effectiveness on the desired output. In this work, Design Expert 8.0.5.0 was utilized for DoE implementation, the software of which contain different sub-functions including Box Behnken, Optimal, Central Composite, Historical and User-Defined Data. Herein, the Historical Data design of Response Surface Method (RSM) was used to perform statistical model establishment, since no constrain on the number of the design factors is required. Before constructing the RSM model, fuel types, PAR and SOI were chosen

as independent variables, which were defined as A, B, C items, respectively (Engine load effect was not considered in the model, the reason of which is discussed in Section 3.4.); while the predicted target responses were ITE performance, NOx and PM emissions, which were defined as Y items. The RSM simulations were carried out based on 48 formal engine tests (3 points of A (three fuels) × 4 points of B (0 - 40%) × 4 points of C (16 - 21 °CA BTDC)). The independent variables of SOI and PAR were coded to (-1, 1), while fuel types (FT, RP-3, Diesel) were coded to (-1, 0, 1) with the arbitrary unit. Besides, the 12 validation engine tests 12 (3 points of A (three fuels) × 2 points of B (10%, 35%) × 2 points of C (17, 20 °CA BTDC)) which were not adopted for RSM model construction, have been used to validate the model prediction performance. Table 5 shows the variables for RSM in both un-coded and coded ranges.

Table 5. The coding of independent variables.

Model Establishment (48 tests)	Code	Units	Un-coded range	Coded range
Fuel types	A	Arbitrary unit	(Diesel, RP-3, FT)	(-1, 0, 1)
PAR	B	%	0 - 40	(-1, 1)
SOI	C	°CA BTDC	16 - 21	(-1, 1)
Engine load	@ 8 bar IMEP			
Model validation (12 tests)	A (Diesel, RP-3, FT) × B (10%, 35%) × C (17, 20 °CA BTDC)			

In the ANOVA analysis, *F*-test has been implemented, in which the *F*-value and *p*-value were obtained to evaluate whether the investigated variables have significant influences on the target's responses. The *F*-test, constructed by a ratio of two different data variability, is performed via the following equation [35] as

$$F = \frac{\text{between-group variability}}{\text{inherent-group variability}} \quad \text{Eq. (8)}$$

The "between-group variability" is derived from

$$\Sigma n_k(\overline{Y_k} - \overline{Y})^2/(K-1) \quad \text{Eq. (9)}$$

where $\overline{Y_k}$ represents the sample average in the k^{th} group, n_k is the observation number in the k^{th} group, $\overline{Y}$ represents the overall average of the collected sample, and T represents the groups number. The "inherent-group variability" is derived from

$$\sum_{kl}(Y_{kl} - \overline{Y}_k)^2/(N-T) \quad \text{Eq. (10)}$$

where Y_{kl} is the l^{th} observation in the k^{th} out of T groups, and N is the whole size of the collected sample.

In this test, $H0$ describes that the input variables do not affect the output responses. If $H0$ is true, then the two measures of both "between-group variability" and "inherent-group variability" will be close to each other, making the ratio nearly 1. If $H0$ is false, the "between-group variability" will be larger than the "inherent-group variability", leading to a ratio larger than 1. As such, a large F - value indicates that the variability depicted by the derived model (Regressions) is greater than the variability inside the process (Residuals). Meanwhile, the p- value denotes the occurrence probability of F statistic based on $H0$ hypothesis. Then, $p <$

0.05 indicates *H*0 can be rejected, and the test results are statistically significant, which means the RSM model is well established with no "Lack of Fit". Additionally, a larger *R*-squared value (the ratio between the model residual and the replicated variability) demonstrates a more statistically significant connection of the input variables and the output responses, further implying the accuracy of the derived model.

3. Results and discussions

3.1 In-cylinder pressure and HRR patterns

In-cylinder data analysis is one of the most effective methods to provide valuable information of combustion characteristics that have direct impacts on engine performance and engine-out pollutants. Herein, Fig. 2 depicts the variations of in-cylinder pressure and HRR of the three test fuels under different SOI, PAR and engine load variables, respectively.

In Fig. 2 (a), SOI was the only variable, changing among 16 °CA， 18 °CA， 19 °CA, and 21 °CA BTDC, while the engine was maintained at the medium load of 4 bar IMEP, and no pentanol was blended in the fuels tested. In other words, the combustion phases were significantly varied by altering SOI for all the test fuels. As SOI advanced, the maximum in-cylinder pressure rose incessantly and occurred closer to the top dead center (TDC). Noticeably, baseline diesel showed an advancement of the maximum heat release as compared to RP-3 kerosene and FT fuel under the same SOI (the combustion phase of maximum HRRs were 6-11 °CA, 8-13 °CA and 11-15 °CA after TDC for baseline diesel, RP-3 kerosene and FT fuel, respectively). There are three reasons, 1) diesel fuel is characterized by higher CN; 2) diesel fuel is also characterized by higher bulk modulus and viscosity, leading to its prominent advancement in the start of combustion; 3) RP-3 kerosene and FT fuel are featured with higher latent heat. Hence, a longer prerequisite time is required for forming well-premixed mixtures, and their ignition delay is postponed compared to baseline diesel.

Further experiments were conducted by varying PAR to investigate its influences on the combustion and emission characteristics. Herein, PAR varied at four test conditions of 0%, 15%, 30% and 40%, respectively, as displayed in Fig. 2 (b). SOI was fixed at 21 °CA BTDC, as the highest ITE was attained at this point (as discussed in the above section), and engine load was maintained at a medium level of 4 bar IMEP. It can be observed that the maximum HRR of baseline diesel experienced an increment from 89.6 to 130.1 kJ/(m^3·deg) as PAR increased from 0% to 40%. Since pentanol has a high resistance to auto-ignition owing to its low CN characteristic, increasing pentanol fraction would gradually prolong the ignition delay. Thus, a better homogeneous charge is formed, enhancing the heat release intensity. Such a trend became even more noticeable for RP-3 kerosene and particularly FT fuel as pentanol fraction increased (increases from 103.8 to 150.7 kJ/(m^3·deg) and 108.3 to 157.2 kJ/(m^3·deg) as PAR increased from 0% to 40%, respectively). Moreover, owing to the significantly promoted homogeneous combustion with a reduced combustion duration as blending pentanol, the slopes of HRR of the aviation fuels, especially the FT type, were much steeper than the baseline diesel.

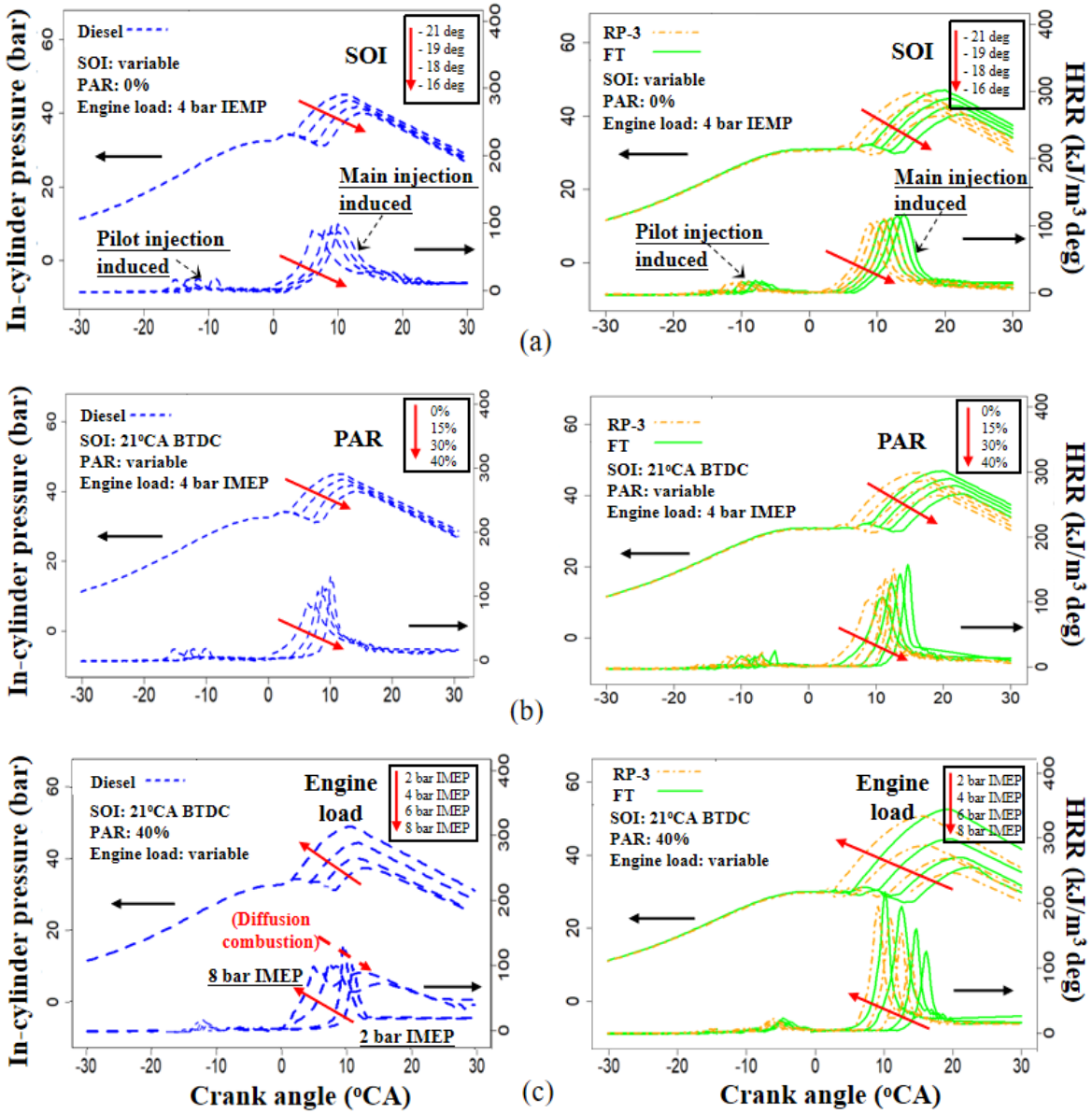

Figure 2. In-cylinder pressure and HRR patterns vs. the variations of SOI (a), PAR (b) and engine loads (c), respectively. The increasing initiation of HRR by the main fuel injection was advanced with the increased engine load.

As displayed in Fig. 2(c), this study was extended further to investigate load effect, in which engine load was varied at 2.0, 4.0, 6.0 and 8.0 bar IMEP for all the test fuels while SOI was fixed at 21 °CA BTDC and PAR was 40% where the highest ITE was attained (as above discussion). Generally, in-cylinder pressure and HRR increased notably as engine load elevating (maximum in-cylinder pressures of baseline diesel, RP-3 kerosene, FT fuel increased from 37 to 48 bar, 39 to 54 bar and 41 to 56 bar, respectively; maximum HRRs of RP-3 kerosene and FT fuel increased from 120.6 to 190.8 kJ/(m^3·deg) and 122.8 to 213.0 kJ/(m^3·deg), respectively). Since higher fuel injection was required as load increased, it caused a larger equivalence ratio, leading to intenser combustion. Whereas, the maximum HRR of baseline diesel experienced a decline as engine load increased over 4 bar IEMP (maximum HRR decreased from 130.1 to 97.4 kJ/(m^3·deg as engine load increased from 4 bar to 8 bar IMEP). As seen in Fig. 2(c), bimodal peaks of the HRR were observed at high load conditions for diesel, demonstrating the occurrence of diffusion combustion, which can deteriorate the in-cylinder combustion status and thus lower the maximum HRR.

3.2 Ignition delay and combustion duration characteristics

Figure 3 (a) displays the results of ignition delay and combustion duration of the three fuels under SOI variation while other operational variables were fixed. Both ignition delay and combustion duration of all the fuels tested demonstrated inappreciable change with the SOI advancement. For instance, as for baseline diesel, ignition delay varied slightly between 8.0 - 8.6 ºCA, and combustion duration varied indistinctively between 23.8 - 25.0 ºCA. These characteristics of different fuels were differentiated from each other under the same SOI. The longest ignition delay was observed for the FT fuel (13.0 - 13.9 ºCA), followed by RP-3 kerosene (11.0 - 11.9 ºCA), and then baseline diesel (8.0 - 8.6 ºCA). The longest combustion duration was found for baseline diesel (23.8-25.0 ºCA), followed by RP-3 kerosene (16.5 - 18.0 ºCA), and then the FT fuel (13.5 - 14.9 ºCA). These aviation fuels were characterized by longer ignition delay and shorter combustion duration: 1) the longer ignition delay for aviation fuels particularly the FT type is due to the lower CN ($CN_{FT} = 40.2 < CN_{RP-3} = 42.0 < CN_{Diesel} = 56.5$) and the higher latent heat (L), which thus leads the temperature reduction during injection ($L_{FT} = 291$ kJ/kg > $L_{RP-3} = 282$ kJ/kg > $L_{diesel} = 270$ kJ/kg); 2) the shorter combustion duration for aviation fuels is because the air-fuel premixing is more sufficient with a longer ignition delay and higher fuel volatility.

Figure 3 (b) shows the variations of ignition delay and combustion duration of the three test fuels under PAR variation as other operational variables remained fixed. The blending of pentanol into the target fuels with different drop-in ratios significantly varied the in-cylinder combustion characteristics. The ignition delay increased remarkably as PAR increased from 0% to 40%, specifically, an increase of 5.0 ºCA, 4.0 ºCA and 3.9 ºCA for baseline diesel, RP-3 kerosene and the FT fuel, respectively. On the contrary, combustion duration decreased notably with the corresponding increment of PAR, causing a decrease of 7.0 ºCA, 6.0 ºCA, and 5.8 ºCA for baseline diesel, RP-3 kerosene and FT fuel, respectively. The blending of pentanol into the target fuels with different drop-in ratios significantly varied the in-cylinder combustion characteristics. This is because pentanol is characterized by a very lower CN ($CN_{pentanol} = 22.5$). The extended ignition delay due to blending pentanol into diesel fuels has been reported in the previous studies [38, 39]. Kumar et al. [18] observed only up to 2.5 ºCA longer ignition delay if the blend ratio of pentanol in diesel was extended from 0% - 45%, which is not as significant compared to the present work. The injection strategy in the present work is with primary injection, so the thermal environment in the cylinder during main injection events is quite different from that in single injection cases. The different ignition delay extension with blending pentanol could be attributed to the different thermal environment during main injection events.

Figure 3 (c) depicts the ignition delay and combustion duration of three test fuels under different engine loads. Different from the results with SOI and PAR variations, the ignition delay declined noticeably as engine load increased from 2 bar to 8 bar IEMP, resulting in a decrease of 3.2 ºCA, 3.2 ºCA, and 3.3 ºCA for baseline diesel, RP-3 kerosene and FT fuel, respectively. On the other hand, the combustion duration increased significantly with the corresponding engine load elevation, resulting in an increase of 13.0 ºCA, 8.0 ºCA and 7.8 ºCA for baseline diesel, RP-3 kerosene and FT fuel, respectively. As engine load increased, in-cylinder temperature elevated, causing an earlier fuel ignition.

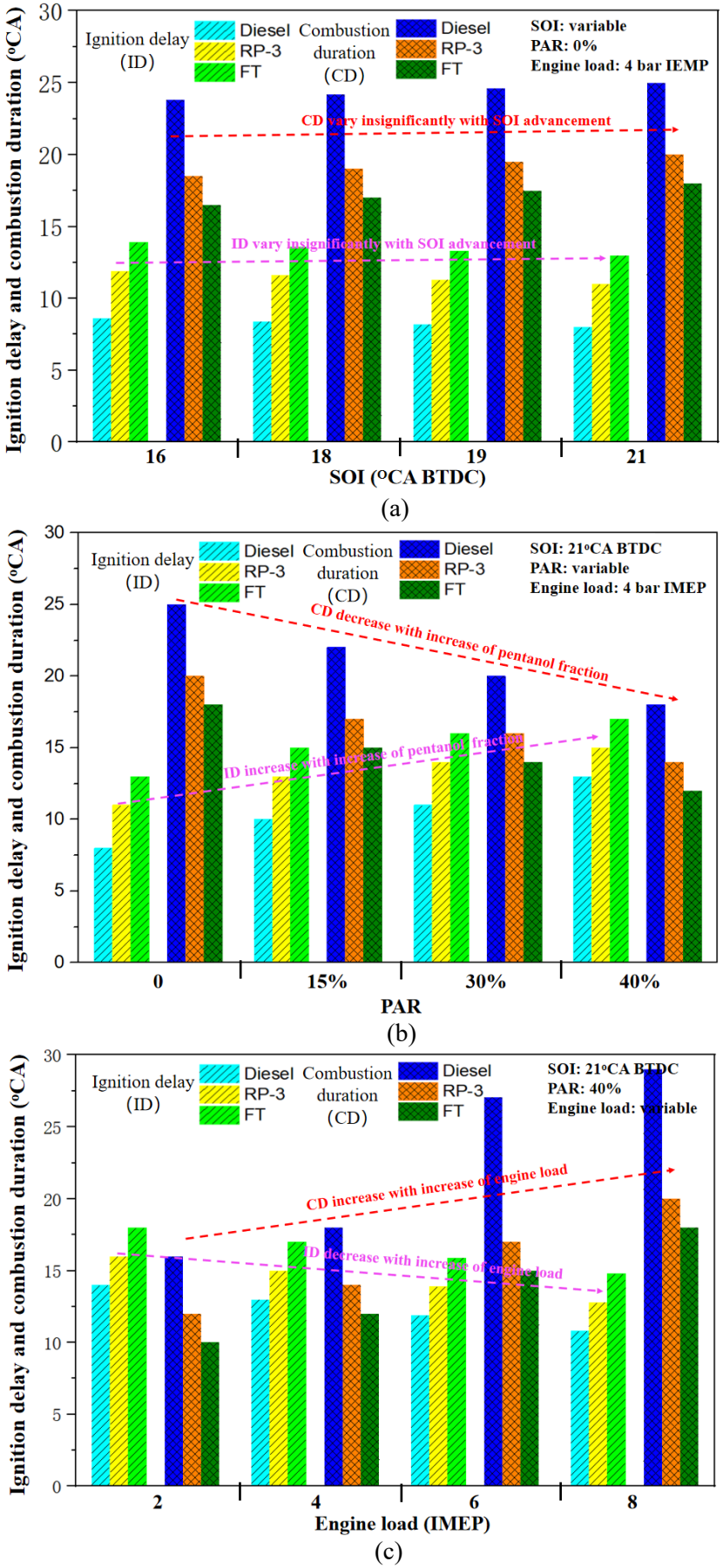

Figure 3. Ignition delay and combustion duration characteristics vs. the variations of SOI (a), PAR (b) and engine loads (c), respectively.

Meanwhile, larger quantities of fuel injection required longer injection duration, and thus a prolonged combustion duration was needed for burning vaster fuel injected. Noticeably, the combustion duration of diesel increased dramatically as the engine load exceeded 4 bar IMEP. This can be explained by the occurrence of diffusion combustion, which constructs more heterogeneous combustion with lower combustion efficiency and a longer combustion duration. Our observation is different from a previous study performed by Ganesh et al., in which no diffusion combustion was observed as their engine operated at the high load state ($\geqslant$6 bar IMEP) [28]. This difference is probably because in their study, they used a reactivity controlled compression ignition (RCCI) engine strategy, which tends to have higher combustion stability than that of our tests.

3.3 Emission characteristics with ITE performance analysis

Figure 4 shows the characteristics of NOx and PM emissions and ITE engine performance of the three test fuels. The results under SOI variation are shown in Fig. 4 (a). It can be seen that both NOx and ITE increased with the SOI advancement for all the fuels (NOx increases of 0.9 g/kW·h, 1.0 g/kW·h and 1.1 g/kW·h for baseline diesel, RP-3 kerosene and FT fuel, respectively; ITE increases of 1.3%, 1.7% and 1.8% for baseline diesel, RP-3 kerosene and FT fuel, respectively.). On the contrary, PM emissions demonstrated a decrease with the SOI advancement (PM decreases of 0.4 1/m, 0.5 1/m and 0.5 1/m for baseline diesel, RP-3 kerosene and FT fuel, respectively). It is declining because the pressure peak of combustion constantly rose towards TDC as the SOI advanced (see Fig. 2(a)). Then, a greater effective work was produced during the expansion stroke. Owing to the increase of in-cylinder temperature under advanced combustion phasing, more thermal NOx were produced because of the enhanced Zeldovich effect [40]. Improved combustion temperature implemented particle oxidation more effectively, so that the PM formation was inhibited as SOI advanced.

Our study indicate that the fuel type has a significant impact on the NOx and PM emissions as well as ITE performance of the engine operated under the same SOI. For instance, as SOI was 21 °CA BTDC, NOx emissions were the greatest for baseline diesel (3.5 g/kW·h), much higher than those of aviation fuels (2.3 g/kW·h for RP-3 and 1.8 g/kW·h for the FT fuel). Since the combustion phase of aviation fuels was retarded away from TDC intensively compared to the baseline diesel (see Fig. 2 (a)), it caused a lower maximum in-cylinder temperature, which thus disfavored NOx formation. Besides, fuel evaporation and atomiszation were improved as if using RP-3 and FT fuels, leading to a prominent increment of ITE and effective inhibition of PM formation compared to diesel. Notably, because of the absence of PAH compositions in the FT fuel, the adoption of FT fuel reduces the PM emission.

Figure 4 (b) displays the emission patterns of NOx, PM and engine performance of ITE of the three test fuels under PAR variation. NOx emissions decreased significantly as PAR increased from 0% to 40%, that is, a decrease of 0.9 g/kW·h, 1.5 g/kW·h and 1.3 g/kW·h for baseline diesel, RP-3 kerosene and FT fuel, respectively. As pentanol fraction increased, fuel vaporization became more effective, resulting in a broader lean combustion flame zone [23, 24]. Thus, the in-cylinder temperature was reduced, and the thermal NOx formation was restrained. Saravanan et al. found that with the increase of pentanol blending ratio, NOx emissions decrease at low loads and increase at high loads [38]. The lower heating value and higher latent heat value of pentanol result in low combustion temperature during the low and medium load. However, the improved premixing combustion through pentanol addition may result in higher temperature at high load.

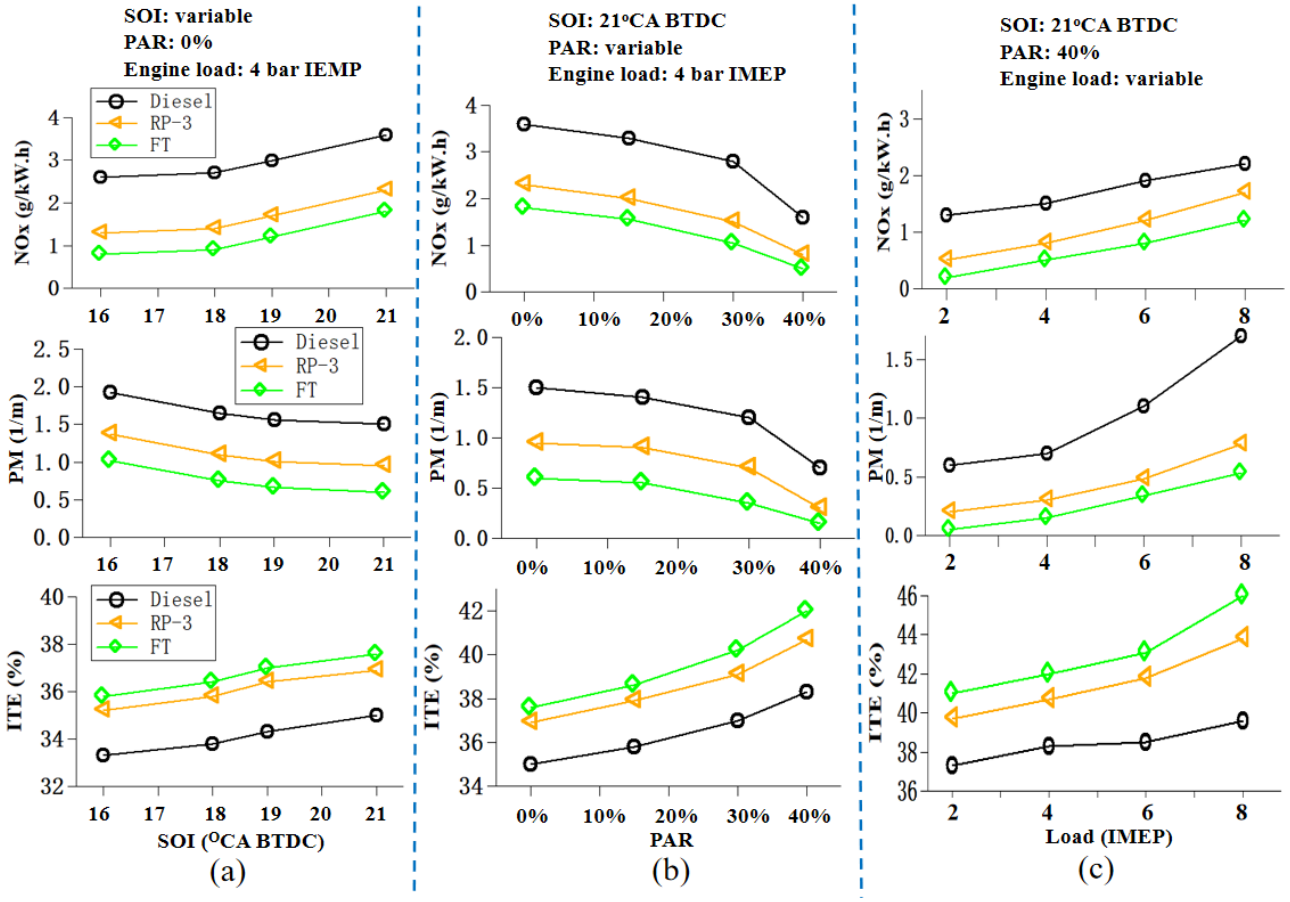

Figure 4. NOx, PM emissions and ITE performance vs. the variations of SOI (a), PAR (b) and engine loads(c), respectively.

The PM emissions also demonstrated a declining trend as PAR increased. This decline can be attributed to three reasons: 1) the oxygen content of pentanol promotes particulate oxidation and also reduces soot nuclei formation. 2) the C/H ratio of pentanol is lower than that of the neat fuels, which lead to a more complete combustion. 3) the addition of pentanol increases the OH concentration via the reaction of methyl radical with HO_2 radical ($CH_3 + HO_2 = CH_3O + OH$), which can further promote particulate oxidation [41]. Additionally, ITE was improved monotonically as PAR increased (3.3%, 3.8% and 4.4% increases for baseline diesel, RP-3 kerosene and FT fuel, respectively) owing to a more complete combustion.

Figure 4 (c) depicts the emission patterns of NOx, PM and engine performance of ITE of the three fuels under engine load variation. As engine load increased from 2 to 8 bar IMEP, both NOx and PM emissions had been prominently elevated with ITE increased concurrently (1.9%, 3.7% and 4.2% increases for baseline diesel, RP-3 kerosene and FT fuel, respectively). As expected, a high load state is attained, and excess air decreases, which favors more pollutants [4, 42]. Noticeably, PM emissions increased aggressively as engine load beyond 4 bar IMEP for baseline diesel (3.5 folds increment from 4 bar to 8 bar IMEP). This is owing to the occurrence of diffusion flame, typically characterized by a wide reaction zone. The over-rich regions are prominent, and high strain rates in the vicinity of the flame front are characterized with fluctuated combustion. Therefore, PM formation is boosted particularly from the locally over-rich burning regions.

3.4 RSM with ANOVA for engine performance and emissions analysis

Based on the polynomial models (transfer functions), RSM in DoE was deployed to determine the cause-effect relationship between the independent variables (fuel types, PAR and SOI) and the target responses (ITE, NOx and PM emissions). Owing to the target responses being the most predominant at 8 bar IMEP load, and the increase of target responses is proportional to the increase of engine load (as seen in Fig. 4 (c)), the RSM analysis were only performed at 8 bar IMEP high load state. Within the RSM model, Y refer to the simulated ITE, NOx and PM emissions; and A, B, C represent the fuel types, PAR and SOI, respectively.

After running the model, the assessments for the modeling results of ITE, NOx and PM are presented in Fig. 5. Figure 5 (a) shows the relation between the normal probability versus internal studentized residuals. The linear distribution of these two parameters implies that the derived models complied with normal distributions [43, 44]. Figure 5 (b) provides the internal studentized residuals scattered around the zero baselines versus various run numbers. The fluctuation indicates that the run number had a tiny probability of causing systematic influence on the derived model. Figure 5 (c) compares the actual values versus the predicted values of the target responses. The linear relation between the experimental and modeling results demonstrates the rationality of the RSM simulations. In addition, another 12 tests have been included to validate the model performance (these test points were not input for model establishment). As seen in Table 6, the R-Squared of the validation points for ITE, NOx and PM are 0.88, 0.85 and 0.82, respectively, which illustrates that the RSM models were successfully established for predicting the target responses. The cost saving can be achieved by reducing the experimental scales based on the effective model prediction.

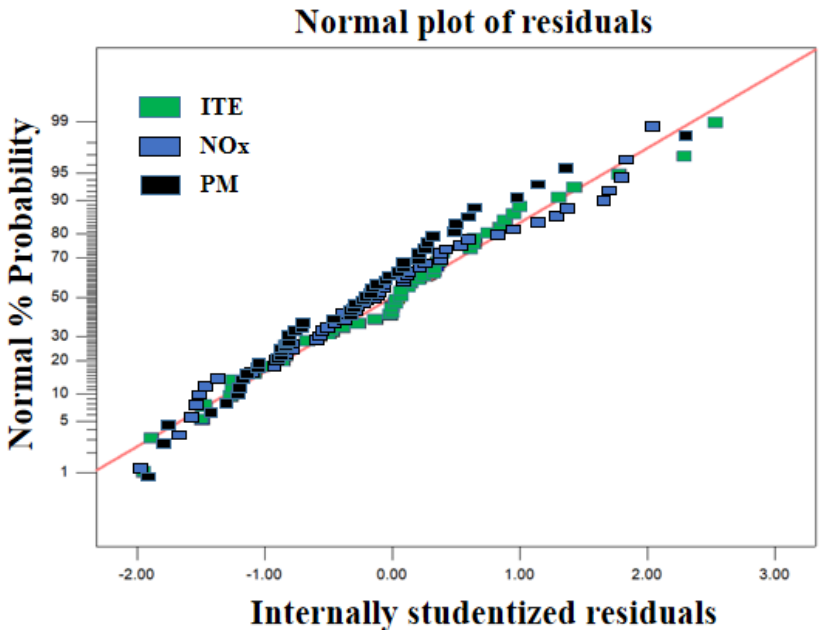

(a)

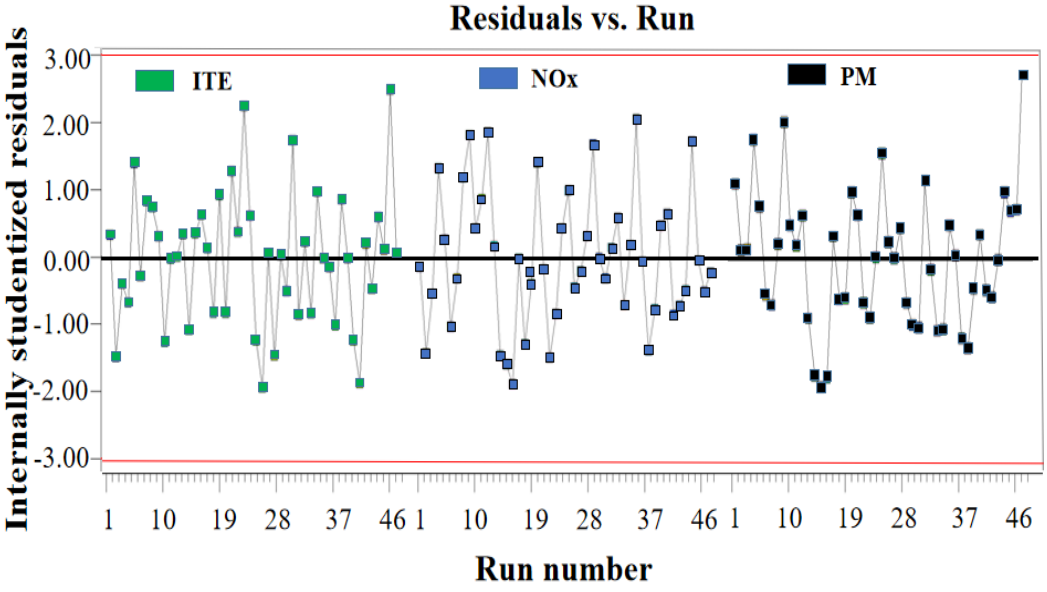

(b)

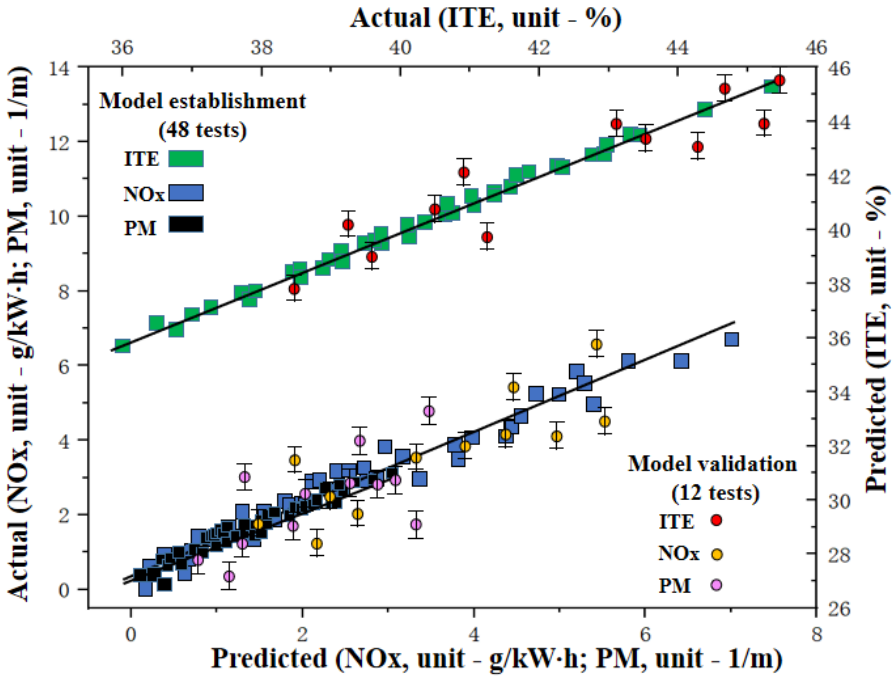

(c)

Figure 5. Assessments on RSM models for ITE, NOx and PM simulations: (a) Normal plot of Residuals, (b) Residuals vs. Run order, (c) Predicted values vs. actual values (48 formal tests for models establishment with 12 additional tests for models validation).

According to Fig. 6 (Simulations of ITE, NOx and PM correlated with fuel types and PAR at fixed SOI (20 ºCA BTDC)), the best ITE was found at the point of (A: FT, B: 40%, C: 20 ºCA BTDC), exhibiting to be 7.2% higher than that of neat diesel (A: Diesel, B: no pentanol, C: SOI 20 ºCA BTDC). Meanwhile, the corresponding NOx and PM emissions were suppressed significantly by 81% and 75%. As seen in Table 6, according to the ANOVA analysis adopted to quantitatively analyze the effectiveness of independent variables on the target responses, the high *F*-values of 575.32, 262.15 and 292.87 (all are $\gg$ 4) for ITE, NOx and PM simulations with *p*-values < 0.01, indicating the sound of RSM derived models [4]. Moreover, the coded

equations of ITE and NOx demonstrate that fuel types were the most dominant factor determining ITE and NOx (A^2 term with the largest coefficients of -1.01 and 1.06 for ITE and NOx, respectively), followed by pentanol fractions (B^2 term with coefficients of 0.74 and -0.96 for ITE and NOx), and then SOI (C term with coefficients of 1.73 and 0.56 for ITE and NOx). Whereas, in terms of PM, pentanol fractions was the primary factor altering the particulate emissions (B^2 term with the largest coefficient of -0.34), followed by fuel types (A^2 term with a coefficient of 0.24), and then SOI (C term with a coefficient of -0.12).

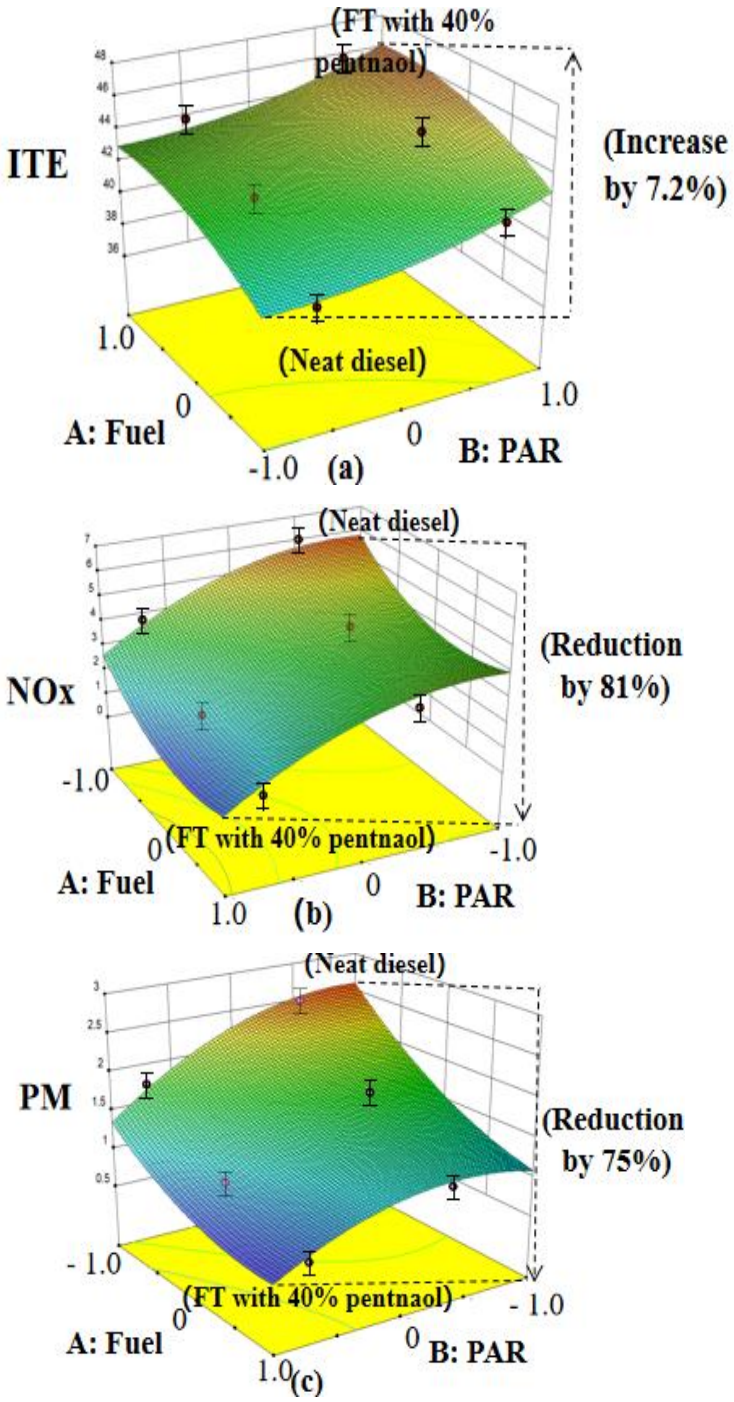

Figure 6. RSM model results of (a) ITE performance (b) NOx emissions (c) and PM emissions correlated with fuel types and PAR at fixed SOI (20 ºCA BTDC). (Engine load is 8 bar IMEP. The circle points of additional tests are for model prediction assessments.)

To illustrate the significant ITE increase, PM and NOx decrease by using pentanol-FT blends, further explanation is given. High pentanol fraction blending into synthetic FT fuel would improve air-fuel premixing compared to conventional fossil fuels. With better air-fuel premixing, the heat release rate is not limited by the fuel diffusion rate but is mainly controlled by the reaction. Thus, the combustion duration is short, and the thermal-to-work conversion is more efficient. Pentanol-FT (40% pentanol) has the lowest CN among all these fuel candidates, so it has the largest ignition delay that is the longest air-fuel premixing duration, and the shortest combustion duration. The longer prerequisite premixing timings facilitates the homogeneous combustion formation, which improves ITE. For emissions characteristics, PM is reduced via burning pentanol-FT because the oxygen content of pentanol promotes particulate oxidation and also reduces soot nuclei formation. In addition, the decrease of NOx is mainly because of the lower heating value and higher latent heat value of the blended fuel. Thus, low combustion temperature restrains the thermal NOx formation. In addition, the simulations of ITE, NOx and PM correlated with SOI and fuel types, and SOI and PAR can be further referred to Fig. S1&S2, respectively.

Table 6. ANOVA analysis on ITE performance, NOx and PM emissions.

Factors	Y(ITE)	Y(NOx)	Y(PM)	
	F-value	*F*-value	*F*-value	*p*-value
Model	575.32	262.15	292.87	< 0.01
A-Fuel types	1137.83	365.15	1041.89	< 0.0001
B-PAR	990.77	812.65	537.12	< 0.0001
C-SOI	1094.45	111.62	9.39	< 0.0001
AB	34.19	-*[1]	54.18	< 0.0038
BC	-*[1]	15.51	-*[1]	< 0.0003
AC	-*[1]	-*[1]	-*[1]	> 0.05
A^2	161.54	173.48	57.93	< 0.0001
B^2	70.57	116.57	100.77	< 0.0001
R-Squared (Model) *[2]	0.98	0.97	0.97	
R-Squared (Validation) *[3]	0.88	0.85	0.82	
Coded Equations:	$Y(ITE) = 42.26+1.56*A+1.54*B+1.73*C+0.27*A*B-1.01*A^2+0.74*B^2$;			
	$Y(NOx) = 2.89-0.89*A-1.43*B+0.56*C-0.27*B*C+1.06*A^2-0.96*B^2$;			
	$Y(PM) = 1.55-0.58*A-0.45*B-0.12*C+0.17*A*B+0.24*A^2-0.34*B^2$			

*[1] represents the item with a *p*-value > 0.05.

*[2] represents the R-Squared of the model results (produced by 48 formal tests).

*[3] represents the R-Squared of the validations (produced by 12 additional tests).

Besides, the RSM method is capable of illustrating the binary and interactive effects of the independent variables on the target responses, as illustrated in Fig. 6. The curvature of the response surfaces indicates the interactive effects of the dual factors concerned. In particular, the strongly curved surfaces in Fig. 6 (a,c) reflect that fuel types (A) and PAR (B) had significantly interactive effects on ITE and PM emissions (AB term of Y(ITE) and Y(PM) had *F*-values of 34.19 and 54.18 with *p*-values < 0.01). The intensively curved surface in Fig. S2 (b) reveals that pentanol fractions (B) and injection timing (C) had greatly coupling effects on NOx emissions (BC term of Y (NOx) had *F*-value of 15.51 with *p*-value < 0.01). The ANOVA analysis demonstrates that the proposed models and all the individual and interaction terms of the models were statistically significant with no 'Lack of Fit'.

4. Conclusions

General aviation aircraft equipped with APE burning heavy fuels (diesel or kerosene) have gained a broad range of applications due to their superior airworthiness, stability and promotional fuel economy. It is desirable to seek promising alternative fuels to promote the comparatively poor combustion and emission characteristics of general aviation in light of the increasingly stringent regulations. In this work, fossil RP-3 kerosene, alternative aviation synthetic FT fuel, baseline diesel and their pentanol blends have been studied on an aviation compression ignition engine. Through systematic experimentation and comprehensive analysis, major conclusions are obtained:

1) At high engine load, diffusion combustion with low heat release rate and long combustion duration occurs for diesel fuel. The RP-3 kerosene and synthetic FT, particularly blended with pentanol, can suppress the occurrence of diffusion combustion effectively, owing to a more homogeneous combustion.

2) The pentanol-FT fuel (40% pentanol) could prominently increase ITE (7.2% promotion) with dramatic suppression on NOx (81% reduction) and PM (75% reduction) compared to neat diesel under 8 bar IMEP engine load.

3) The non-linear RSM DoE models have quantified the effects of fuel types, PAR and SOI on ITE, NOx and PM responses. It shows that fuel types predominantly determined ITE and NOx, while pentanol fractions primarily determined PM emissions (model *F*-values$\gg$4).

4) Binary and interactive effects of the operational variables on the engine performance/emission characteristics were quantitatively resolved by ANOVA (model *p*-values<0.05).

5) The RSM models have been validated to be capable of predicting engine performance/emission characteristics properly (R-Squared of ITE, NOx and PM in simulation validation are 0.88, 0.85 and 0.82, respectively).

Acknowledgments

This work was supported by China Scholarship Council (NO. 201905064). This work was also supported by the National Natural Science Foundation of China (51922019 & 51920105009). Valuable guidance from Prof. Hongming Xu at the University of Birmingham is gratefully acknowledged.

Supporting information

Supplemental data associated with this article can be found, in the online version.

References

[1] Marsh G. Airbus A350 XWB update. Reinforced Plastics. 2010;54(6):20-4.

[2] Turgut ET, Açıkel Gr, Gaga EO, Calisir D, Odabasi M, Ari A, et al. A comprehensive characterization of particulate matter, trace elements, and gaseous emissions of piston-engine aircraft. Environmental Science & Technology. 2020;54(13):7818-35.

[3] Rindlisbacher T. Aircraft piston engine emissions summary report. Switzerland: Federal Department of the Environment, Transport, Energy and Communications & Federal Office of Civil Aviation, Aviation Policy and Strategy Environmental Affairs. 2007.

[4] Chen L, Liang Z, Liu H, Ding S, Li Y. Sensitivity analysis of fuel types and operational parameters on the particulate matter emissions from an aviation piston engine burning heavy fuels. Fuel. 2017;202:520-8.

[5] Masiol M, Harrison RM. Aircraft engine exhaust emissions and other airport-related contributions to ambient air pollution: A review. Atmospheric Environment. 2014;95:409-55.

[6] Liang Z, Yu Z, Zhang C, Chen L. IVOC/SVOC and size distribution characteristics of particulate matter emissions from a modern aero-engine combustor in different operational modes. Fuel. 2021:122781.

[7] Fernandes G, Fuschetto J, Filipi Z, Assanis D, McKee H. Impact of military JP-8 fuel on heavy-duty diesel engine performance and emissions. Proceedings of the Institution of Mechanical Engineers, Part D: Journal of Automobile Engineering. 2007;221(8):957-70.

[8] Olfert JS, Dickau M, Momenimovahed A, Saffaripour M, Thomson K, Smallwood G, et al. Effective density and volatility of particles sampled from a helicopter gas turbine engine. Aerosol Science and Technology. 2017;51(6):704-14.

[9] Chen L, Ding S, Liu H, Lu Y, Li Y, Roskilly AP. Comparative study of combustion and emissions of kerosene (RP-3), kerosene-pentanol blends and diesel in a compression ignition engine. Applied Energy. 2017;203:91-100.

[10] Turgut ET, Gaga EO, Jovanović G, Odabasi M, Artun G, Ari A, et al. Elemental characterization of general aviation aircraft emissions using moss bags. Environmental Science Pollution Research. 2019;26(26):26925-38.

[11] Lobo P, Hagen DE, Whitefield PD. Comparison of PM emissions from a commercial jet engine burning conventional, biomass, and Fischer–Tropsch fuels. Environmental Science & Technology. 2011;45(24):10744-9.

[12] Drozd GT, Miracolo MA, Presto AA, Lipsky EM, Riemer DD, Corporan E, et al. Particulate matter and organic vapor emissions from a helicopter engine operating on petroleum and Fischer–Tropsch fuels. Energy & Fuels. 2012;26(8):4756-66.

[13] Morón-Villarreyes JA, Soldi C, de Amorim AM, Pizzolatti MG, de Mendonça Jr AP, Doca MG. Diesel/biodiesel proportion for by-compression ignition engines. Fuel. 2007;86(12-13):1977-82.

[14] Gill S, Tsolakis A, Dearn K, Rodríguez-Fernández. Combustion characteristics and emissions of Fischer–Tropsch diesel fuels in IC engines. Progress in Energy Combustion Science. 2011;37(4):503-23.

[15] Defense Standard. Turbine fuel, Aviation Kerosene Type, Jet A-1 NATO Code: F-35 Joint Service Designation:

AVTUR. Ministry of Defence, 2008. 30.

[16] Corporan E, Edwards T, Shafer L, DeWitt MJ, Klingshirn C, Zabarnick S, et al. Chemical, thermal stability, seal swell, and emissions studies of alternative jet fuels. Energy & Fuels. 2011;25(3):955-66.

[17] Corporan E, DeWitt MJ, Klingshirn CD, Anneken D, Shafer L, Streibich R. Comparisons of emissions characteristics of several turbine engines burning Fischer-Tropsch and hydroprocessed esters and fatty acids alternative Jet fuels. American Society of Mechanical Engineers. 425-36.

[18] Kumar BR, Saravanan S. Use of higher alcohol biofuels in diesel engines: A review. Renewable and Sustainable Energy Reviews. 2016;60:84-115.

[19] Ashok B, Jeevanantham A, Nanthagopal K, Saravanan B, Kumar MS, Johny A, et al. An experimental analysis on the effect of n-pentanol-calophyllum inophyllum biodiesel binary blends in CI engine characteristcis. Energy. 2019;173:290-305.

[20] Balan K, Yashvanth U, Booma Devi P, Arvind T, Nelson H, Devarajan Y. Investigation on emission characteristics of alcohol biodiesel blended diesel engine. Energy Sources, Part A: Recovery, Utilization, Environmental Effects. 2019;41(15):1879-89.

[21] Bhowmik S, Panua R, Debroy D, Paul A. Artificial neural network prediction of diesel engine performance and emission fueled with diesel–kerosene–ethanol blends: a fuzzy-based optimization. Journal of Energy Resources Technology. 2017;139(4).

[22] Huang Z, Lu H, Jiang D, Zeng K, Liu B, Zhang J, et al. Combustion behaviors of a compression-ignition engine fuelled with diesel/methanol blends under various fuel delivery advance angles. Bioresource Technology. 2004;95(3):331-41.

[23] Li L, Wang J, Wang Z, Xiao J. Combustion and emission characteristics of diesel engine fueled with diesel/biodiesel/pentanol fuel blends. Fuel. 2015;156:211-8.

[24] Li L, Wang J, Wang Z, Liu H. Combustion and emissions of compression ignition in a direct injection diesel engine fueled with pentanol. Energy. 2015;80:575-81.

[25] Babu V, Murthy M. Butanol and pentanol: The promising biofuels for CI engines–A review. Renewable Sustainable Energy Reviews. 2017;78:1068-88.

[26] Wang J, Wu F, Xiao J, Shuai S. Oxygenated blend design and its effects on reducing diesel particulate emissions. Fuel. 2009;88(10):2037-45.

[27] Panneerselvam N, Murugesan A, Vijayakumar C, Kumaravel A, Subramaniam D, Avinash A. Effects of injection timing on bio-diesel fuelled engine characteristics—an overview. Renewable and Sustainable Energy Reviews. 2015;50:17-31.

[28] Ganesh D, Ayyappan P, Murugan R. Experimental investigation of iso-butanol/diesel reactivity controlled compression ignition combustion in a non-road diesel engine. Applied Energy. 2019;242:1307-19.

[29] Sayin C, Ilhan M, Canakci M, Gumus M. Effect of injection timing on the exhaust emissions of a diesel engine using diesel–methanol blends. Renewable Energy. 2009;34(5):1261-9.

[30] Gopinath S, Devan P, Mohan C, Prasad SV. A review on influence of injection timing and injection pressure on DI diesel engine fuelled with low viscous fuel. Materials Today: Proceedings. 2020;33:280-6.

[31] Kockal NU, Ozturan T. Optimization of properties of fly ash aggregates for high-strength lightweight concrete production. Materials Design. 2011;32(6):3586-93.

[32] Sahu J, Acharya J, Meikap B. Response surface modeling and optimization of chromium (VI) removal from

aqueous solution using Tamarind wood activated carbon in batch process. Journal of Hazardous Materials. 2009;172(2-3):818-25.

[33] Chen L, Liu Z, Sun P, Huo W. Formulation of a fuel spray SMD model at atmospheric pressure using Design of Experiments (DoE). Fuel. 2015;153:355-60.

[34] Li Z, Lu D, Gao X. Multi-objective optimization of gap-graded cement paste blended with supplementary cementitious materials using response surface methodology. Construction Building Materials. 2020;248:118552.

[35] Chen L, Ma Y, Guo Y, Zhang C, Liang Z, Zhang X. Quantifying the effects of operational parameters on the counting efficiency of a condensation particle counter using response surface Design of Experiments (DoE). Journal of Aerosol Science. 2017;106:11-23.

[36] Cheikh K, Sary A, Khaled L, Abdelkrim L, Mohand T. Experimental assessment of performance and emissions maps for biodiesel fueled compression ignition engine. Applied Energy. 2016;161:320-9.

[37] Atmanli A, Ileri E, Yuksel B, Yilmaz N. Extensive analyses of diesel–vegetable oil–n-butanol ternary blends in a diesel engine. Applied Energy. 2015;145:155-62.

[38] Kumar BR, Saravanan S. Effect of exhaust gas recirculation (EGR) on performance and emissions of a constant speed DI diesel engine fueled with pentanol/diesel blends. Fuel. 2015;160:217-26.

[39] Wei L, Cheung CS, Huang Z. Effect of n-pentanol addition on the combustion, performance and emission characteristics of a direct-injection diesel engine. Energy. 2014;70:172-80.

[40] Fu Z, Gao H, Zeng Z, Liu J, Zhu Q. Generation characteristics of thermal NOx in a double-swirler annular combustor under various inlet conditions. Energy. 2020;200:117487.

[41] Liu Y, Liggio J, Harner T, Jantunen L, Shoeib M, Li S-M. Heterogeneous OH initiated oxidation: a possible explanation for the persistence of organophosphate flame retardants in air. Environmental Science & Technology. 2014;48(2):1041-8.

[42] Liu H, Wang Z, Wang J, He X, Zheng Y, Tang Q, et al. Performance, combustion and emission characteristics of a diesel engine fueled with polyoxymethylene dimethyl ethers (PODE3-4)/diesel blends. Energy. 2015;88:793-800.

[43] Jeirani Z, Jan BM, Ali BS, Noor IM, Hwa SC, Saphanuchart W. The optimal mixture design of experiments: Alternative method in optimizing the aqueous phase composition of a microemulsion. Chemometrics Intelligent Laboratory Systems. 2012;112:1-7.

[44] Khuri AI, Mukhopadhyay S. Response surface methodology. Wiley Interdisciplinary Reviews: Computational Statistics. 2010;2(2):128-49.